Title
Nanoparticle-Driven Assembly of Highly Conducting Hybrid Block Copolymer Electrolytes

Journal
Macromolecules, 48(2)

ISSN
0024-9297

Authors
Villaluenga, Irune
Chen, Xi Chelsea
Devaux, Didier
et al.

Publication Date
2015-01-27

DOI
10.1021/ma502234y

Peer reviewed

Macromolecules

Article

pubs.acs.org/Macromolecules

Nanoparticle-Driven Assembly of Highly Conducting Hybrid Block Copolymer Electrolytes

Irune Villaluenga,[†,⊥] Xi Chelsea Chen,[‡] Didier Devaux,[†] Daniel T. Hallinan,[§] and Nitash P. Balsara*[,†,‡,∥,⊥]

[†]Environmental Energy Technologies Division, [∥]Materials Sciences Division, and [⊥]Joint Center for Energy Storage Research (JCESR), Lawrence Berkeley National Laboratory, Berkeley, California 94720, United States

[‡]Department of Chemical and Biomolecular Engineering, University of California, Berkeley, California 94720, United States

[§]Department of Chemical and Biomedical Engineering, Florida State University, Tallahassee, Florida 32310-6046, United States

ABSTRACT: Hybrid nanostructured materials comprising block copolymers, nanoparticles, and lithium salts have the potential to serve as electrolytes in non-flammable rechargeable lithium batteries. Here we show that the addition of functionalized nanoparticles, at an optimized concentration, into lamellar block copolymer electrolytes, results in an increase in ionic conductivity. This is due to the occurrence of a lamellar-to-bicontinuous phase transition, driven by the addition of nanoparticles. The magnitude of the increase in conductivity is consistent with a simple model that accounts for the morphology of the conducting channels. The conductivity of the optimized hybrid electrolyte is only 6% lower than that of an idealized nanostructured electrolyte with perfectly connected conducting pathways and no dead ends.

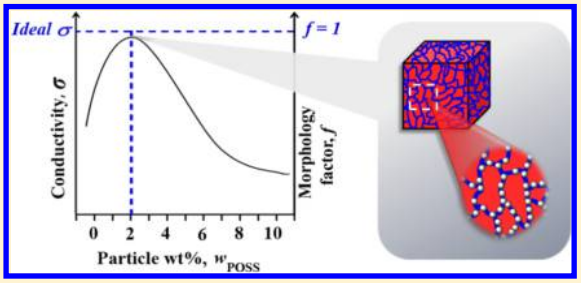

1. INTRODUCTION

Electrolytes used in rechargeable lithium batteries are mixtures of lithium salts and alkyl carbonate solvents. The high ionic conductivity of these electrolytes is well-suited for several applications including cellphones and laptops. Unfortunately, these electrolytes are flammable, and this limits our ability to use lithium batteries in large devices like electric vehicles. Solid polymer electrolytes are inherently less flammable and thus better suited for large applications.[1−4] The use of high modulus solid polymer electrolytes may also enable the design of higher specific energy lithium batteries with lithium metal anodes.[5]

Block copolymers self-assembly into different morphologies such as lamellae, bicontinuous gyroid networks, cylinders arranged on a hexagonal lattice, and spheres arranged on a body-centered-cubic lattice.[6] Electrolytes comprising mixtures of polystyrene−*b*-poly(ethylene oxide) (SEO) block copolymers and lithium salts can, in principle, enable independent control over electrical and mechanical properties. In these systems, the conductive pathways are provided by poly(ethylene oxide)-rich microphase, while the non-conducting polystyrene-rich microphase imparts the desired mechanical properties. The ionic conductivity of block copolymer electrolytes, $\sigma(T)$, is often expressed as:[7−10]

$$\sigma(T) = f\phi_c\sigma_c(T) \quad (1)$$

where f is the morphology factor that accounts for the geometry and connectivity of the conducting phase, $\sigma_c(T)$ is the intrinsic conductivity of the conducting phase, and ϕ_c is the volume fraction of the conducting phase. In this work, we restrict our attention to samples containing randomly oriented grains.

Theoretical work of Sax and Ottino on transport through heterogeneous media[11] enables calculations of the dependence of f on electrolyte morphology. We refer to these calculated values as f_{ideal}. The results of these calculations for a selected set of morphologies are presented in Figure 1. Also shown in Figure 1 are schematics of block copolymer grains with conducting (blue) and non-conducting (red) microphases. For the sphere morphology, f_{ideal} is 0 because there are no effective conducting pathways. For the cylinder morphology, f_{ideal} is 1/3 because, on average, only one-third of the grains will contribute to the ion transport in specify direction. For the lamellae morphology, f_{ideal} is 2/3 because, on average, two-thirds of the grains will contribute to the ion transport in specify direction. For the bicontinuous morphology, has a f_{ideal} = 1, i.e, all grain orientations are effective for the ion transport. The morphology factors given in Figure 1 are expected to apply to systems wherein the width of the conducting channels are much larger than the diameter of the diffusing species. Effects such as changes in friction near the wall of the conducting channels and the reduction in the dimensionality of diffusion due to confinement are also not accounted for.

The experimentally determined morphology factors of block copolymer electrolytes reported in the literature are summarized in Table 1. Most of the experimental values are significantly less than f_{ideal}. In principle, bicontinuous morphologies should give the highest values of f, but the

Received: November 3, 2014
Revised: December 23, 2014
Published: January 13, 2015

DOI: 10.1021/ma502234y
Macromolecules 2015, 48, 358−364

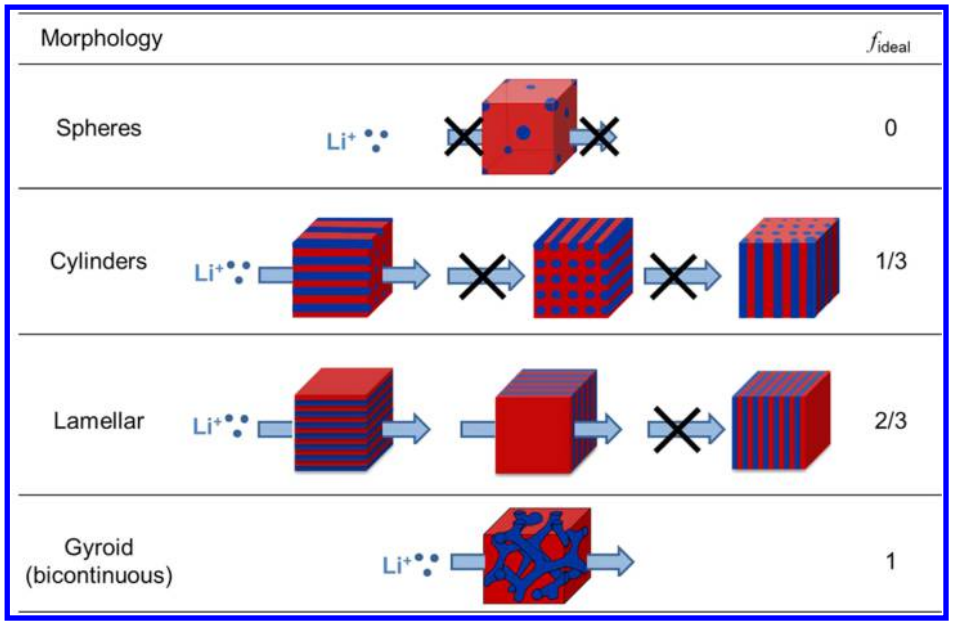

Figure 1. Dependence of the ideal morphology factor, f_{ideal}, on morphology. The blue and red regions represent conducting and non-conducting microphases, respectively.

Table 1. Experimental Determined Morphology Factor, *f*, of Block Copolymer Electrolytes Taken from the Literature at 90 °C[a]

reference	morphology	electrolyte	f	f_{ideal}
R. L. Weber et al.[12]	cylinders	PS-*b*-PIL	0.03	1/3
N. S. Wanakule et al.[13]	lamellar	PS-*b*-PEO	0.35	2/3
M. Singh et al.[7]	lamellar	PS-*b*-PEO	0.57	2/3
R. L. Weber et al.[12]	lamellar	PS-*b*-PIL	0.44	2/3
M. W. Schulze et al.[14]	disordered bicontinuous	PS-*b*-PEO	0.33−0.66	1
N. S. Wanakule et al.[13]	gyroid (bicontinuous)	PS-*b*-PEO	0.35	1
M. W. Hamersky et al.[15]	gyroid (bicontinuous)	PEE- *b*-PEO	0.66	1

[a]Abbreviations: PS-*b*-PEO, polystyrene-*block*-poly(ethylene oxide); PS-*b*-PIL, polystyrene-*block*-poly(ionic liquid); and PEE-*b*-PEO, polyethylethylene-*block*-poly(ethylene oxide).

literature reports of f obtained from these systems are comparable to those obtained from lamellar samples.

One approach to control the morphology of block copolymer electrolytes is by the addition of nanoparticles. The morphology of these systems depends on the arrangement and the location of the nanoparticles in the block copolymer.[16−20] In particular, Kramer et al. demonstrated nanoparticle-induced phase transitions in block copolymers.[21] They also showed that the location of nanoparticles in the block copolymer domains could be controlled by covering the nanoparticle surfaces with tailored ligands.

In this paper we report on the synthesis and characterization of a hybrid block copolymer electrolyte with $f = 0.94 \pm 0.28$ and an ionic conductivity of $1.05 \times 10^{-3} \pm 4.22 \times 10^{-4}$ S/cm at 90 °C. The electrolytes comprise an SEO copolymer, silsesquioxane nanoparticles, and lithium salt. There are several previous studies on the effect of the addition of nanoparticles on morphology of block copolymers. In our system, the addition of surface-modified silsesquioxane nanoparticles to an SEO electrolyte at an optimized concentration results in a transformation from lamellar to a disordered bicontinuous morphology. The reported value of f is thus very close to f_{ideal}.

2. EXPERIMENTAL SECTION

Materials. *N*,*N*-Dimethylformamide anhydrous (DMF, 99.8%) was purchased from Sigma-Aldrich. Lithium bis(trifluoromethanesulfone)-imide, $Li[N(SO_2CF_3)_2]$ (LiTFSI), was purchased from Novolyte, and polyethylene glycol polyhedral oligomeric silsesquioxane (PEO-POSS) with a chemical formula $(SiO_{1.5})_8(CH_2CH_2O)_{13}CH_3$ was purchased from Hybrid Plastic. All chemicals were used as received. Polystyrene-*block*-poly(ethylene oxide) copolymer (PS: 70 kg/mol and PEO: 74 kg/mol, SEO) was synthesized by sequential anionic polymerization of styrene followed by ethylene oxide using methods described in ref 22.

Hybrid Block Copolymer Samples Preparation. Two kinds of samples were made as summarized in Tables 2 and 3. The synthesis of all samples was carried out in an MBraun glovebox, maintaining an argon atmosphere with ultralow concentrations of water, oxygen, and organic solvents. Salty hybrid block copolymer samples (SEO-LiTFSI-POSS-w_{POSS}) were prepared by mixing PEO-POSS nanoparticles, SEO copolymer, and LiTFSI in dry DMF using a hot plate at 110 °C for 12 h to obtain homogeneous solutions at different weight percentage of the added inorganic nanoparticle, w_{POSS}, with a molar ratio of lithium atoms to ethylene oxide (EO) moieties, r, 0.085 for all samples (Table

Table 2. Characteristics of Non-salty Hybrid Block Copolymers (SEO-POSS-w_{POSS})

name	w_{POSS}	$w_{PEO\text{-}POSS}$	ϕ_{POSS}	$\phi_{PEO\text{-}POSS}$	ϕ_{EO}
SEO-POSS-0	0	0	0	0	0.49
SEO-POSS-2	2	15.88	0.016	0.13	0.54
SEO-POSS-5	5	32.76	0.035	0.23	0.58
SEO-POSS-7	7	41.07	0.047	0.27	0.60
SEO-POSS-10	10	50.71	0.063	0.32	0.62

DOI: 10.1021/ma502234y
Macromolecules 2015, 48, 358−364

Table 3. Characteristics of Salty Hybrid Block Copolymers (SEO-LiTFSI-POSS-w_{POSS})

name	w_{POSS}	$w_{PEO\text{-}POSS}$	ϕ_{POSS}	$\phi_{PEO\text{-}POSS}$	ϕ_{EO}	T_g (°C)
SEO-LiTFSI-POSS-0	0	0	0	0	0.55	−40
SEO-LiTFSI-POSS-2	2	15.88	0.014	0.11	0.59	−44
SEO-LiTFSI-POSS-5	5	32.76	0.032	0.20	0.62	−44
SEO-LiTFSI-POSS-7	7	41.07	0.042	0.25	0.64	−47
SEO-LiTFSI-POSS-10	10	50.71	0.057	0.29	0.65	−47

3). The solutions of material in DMF (10:90 v/v) were cast on an aluminum foil and dried at 90 °C to obtain membranes with thicknesses ranging from 10 to 100 μm. To ensure complete solvent removal, the hybrid block copolymer electrolytes were subsequently dried overnight under vacuum at 90 °C in the glovebox antechamber. The procedure described above was also used to make non-salty hybrid block copolymer samples (SEO-POSS-w_{POSS}) by skipping the salt-addition step. Table 2 lists the salt-free composites studied here. Samples are labeled SEO-POSS-w_{POSS} where w_{POSS} is the weight percentage of the added inorganic nanoparticle. We assume that the salt and PEO-POSS nanoparticles reside almost exclusively in the PEO domain.[23] The weight percentage of EO in the SEO copolymer, $w_{EO(SEO)}$, is calculated from the molecular weight of the PEO block without correcting for end groups. The weight percentage of inorganic content of nanoparticles, w_{POSS}, the weight percentage of EO in the nanoparticles, $w_{EO(PEO\text{-}POSS)}$, and the weight percentage of the added PEO-POSS nanoparticles, $w_{PEO\text{-}POSS}$, are determined by thermogravimetric analysis (TGA). The inorganic content proved to be 10.8 wt % in PEO-POSS nanoparticles. The volume fraction of the conducting phase, ϕ_{EO} (eq 2), the volume fraction of the inorganic content, ϕ_{POSS} (eq 3), and the volume fraction of the added PEO-POSS nanoparticles, $\phi_{PEO\text{-}POSS}$ (eq 4), can be calculated by:

$$\phi_{EO} = \frac{v_{EO} + rv_{LiTFSI} + \frac{w_{EO(PEO\text{-}POSS)}M_{EO}}{w_{EO(SEO)}\rho_{PEO\text{-}POSS}}}{v_{EO} + rv_{LiTFSI} + \frac{w_{PEO\text{-}POSS}M_{EO}}{w_{EO(SEO)}\rho_{PEO\text{-}POSS}} + \frac{M_{PS}M_{EO}}{M_S M_{PEO}}v_S} \quad (2)$$

$$\phi_{POSS} = \frac{\frac{w_{POSS}M_{EO}}{w_{EO(SEO)}\rho_{PEO\text{-}POSS}}}{v_{EO} + rv_{LiTFSI} + \frac{w_{PEO\text{-}POSS}M_{EO}}{w_{EO(SEO)}\rho_{PEO\text{-}POSS}} + \frac{M_{PS}M_{EO}}{M_S M_{PEO}}v_S} \quad (3)$$

$$\phi_{PEO\text{-}POSS} = \frac{\frac{w_{(PEO\text{-}POSS)}M_{EO}}{w_{EO(SEO)}\rho_{PEO\text{-}POSS}}}{v_{EO} + rv_{LiTFSI} + \frac{w_{PEO-POSS}M_{EO}}{w_{EO(SEO)}\rho_{PEO\text{-}POSS}} + \frac{M_{PS}M_{EO}}{M_S M_{PEO}}v_S} \quad (4)$$

where $\rho_{PEO\text{-}POSS}$ is the density of PEO-POSS nanoparticles (1.1 g cm^3), $w_{EO(SEO)}$ is the weight percentage of EO in the SEO copolymer, v_{EO}, v_{LiTFSI}, and v_S are the molar volumes of EO monomer units (41.56 cm^3 mol^{-1}), LiTFSI (141.9 cm^3 mol^{-1}), and styrene monomer units (107.4 cm^3 mol^{-1}), respectively, and M_S and M_{EO} are the molar masses of styrene (104.15 g mol^{-1}) and ethylene oxide (44.05 g mol^{-1}), respectively.[23]

Differential Scanning Calorimetry. The glass transition temperatures (T_g) for the salty samples (SEO-LiTFSI-POSS-w_{POSS}) were obtained from analysis of the second heating run, using differential scanning calorimetry (DSC) experiments (Table 3). Samples were sealed in aluminum hermetic pans in the glovebox. DSC scans were conducted over the temperature range −75 to 150 °C at a rate of 5 °C min^{-1}.

Conductivity Measurements. Symmetrical cells were assembled in the glovebox using the salty hybrid block copolymer samples (SEO-LiTFSI-POSS-w_{POSS}) as electrolytes. The samples were hand-pressed into a pellet and placed at the center of an insulating spacer with a 3.17 mm diameter central hole and heated in a hand press to 100 °C for 10 s. The samples were placed between two mirror-polished nickel electrodes and heated to 100 °C for 5 s in a hand press to ensure good contact between the electrodes and the electrolyte. Nickel current collector tabs are placed on each electrode to assemble the cells. Finally, the symmetrical cell is vacuum sealed in a pouch bag to isolate it from air.

Impedance spectroscopy measurements were performed using a VMP3 (Bio-Logic) with an ac amplitude of 50 mV in the frequency range 1 MHz−1 Hz. Impedance spectra were recorded at 10 °C intervals during heating and cooling scans between 23 and 120 °C. The ionic conductivity of the conducting phase in hybrid electrolytes, $\sigma(T)$, is calculated from the measured sample thickness l and the cross-sectional area S of the spacer, and electrolyte resistance R_{el} was determined by the methods discussed in ref 24. $\sigma(T)$ is given by:

$$\sigma(T) = l/(S^*R_{el}(T)) \quad (5)$$

Morphology Characterization. The morphological characterization of the hybrid block copolymer samples was accomplished by small-angle X-ray scattering (SAXS) and scanning transmission electron microscope (STEM). The samples used for SAXS are both non-salty and salty hybrid block copolymers (SEO-POSS-w_{POSS} and SEO-LiTFSI-POSS-w_{POSS}) that were first annealed at 90 °C for at least 24 h and then sealed inside homemade airtight sample holders with Kapton windows. The samples were sealed off from the surrounding atmosphere by a rubber gasket and screw assembly. The entire sample preparation procedure for SAXS was done inside an argon filled glovebox. The SAXS data were obtained at the Advanced Light Source (ALS) at Lawrence Berkeley National Laboratory, Berkeley, CA, at beamline 7.3.3. The hybrid block copolymer samples for STEM were prepared without LiTFSI to minimize water contamination in the membranes. Samples were annealed at 90 °C for a minimum of 24 h in vacuum. Thin sections with thicknesses of approximately 70 nm were obtained by cryo-microtoming using a Leica EM FC6 and picked up on a lacey carbon coated copper grid (Electron Microscopy Sciences). STEM experiments were performed on a Tecnai F20 UT FEG, equipped with a high angle annular dark field (HAADF) detector, using 200 keV acceleration voltage.

3. RESULTS AND DISCUSSION

The dependence of the ionic conductivity of the hybrid block copolymer electrolytes, σ, on temperature and nanoparticle loading is shown in Figure 2. Conductivity increases when the particle loading is increased from 0 to 2 wt % but decreases as

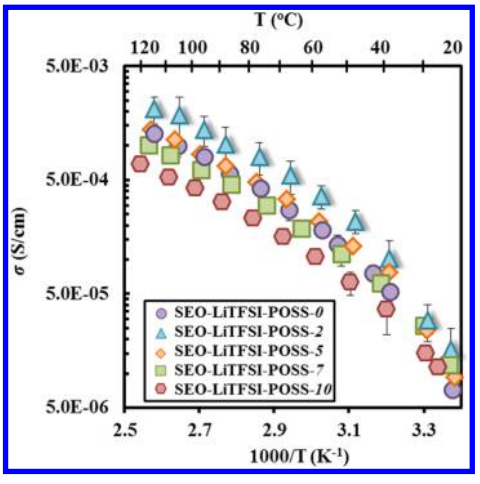

Figure 2. Ionic conductivity, σ, of salty hybrid block copolymer samples (SEO-LiTFSI-POSS-w_{POSS}) versus the temperature, w_{POSS} is weight % of the inorganic portion of the nanoparticles. In many cases, the size of the error bar is smaller than the size of the data points.

DOI: 10.1021/ma502234y
Macromolecules 2015, 48, 358−364

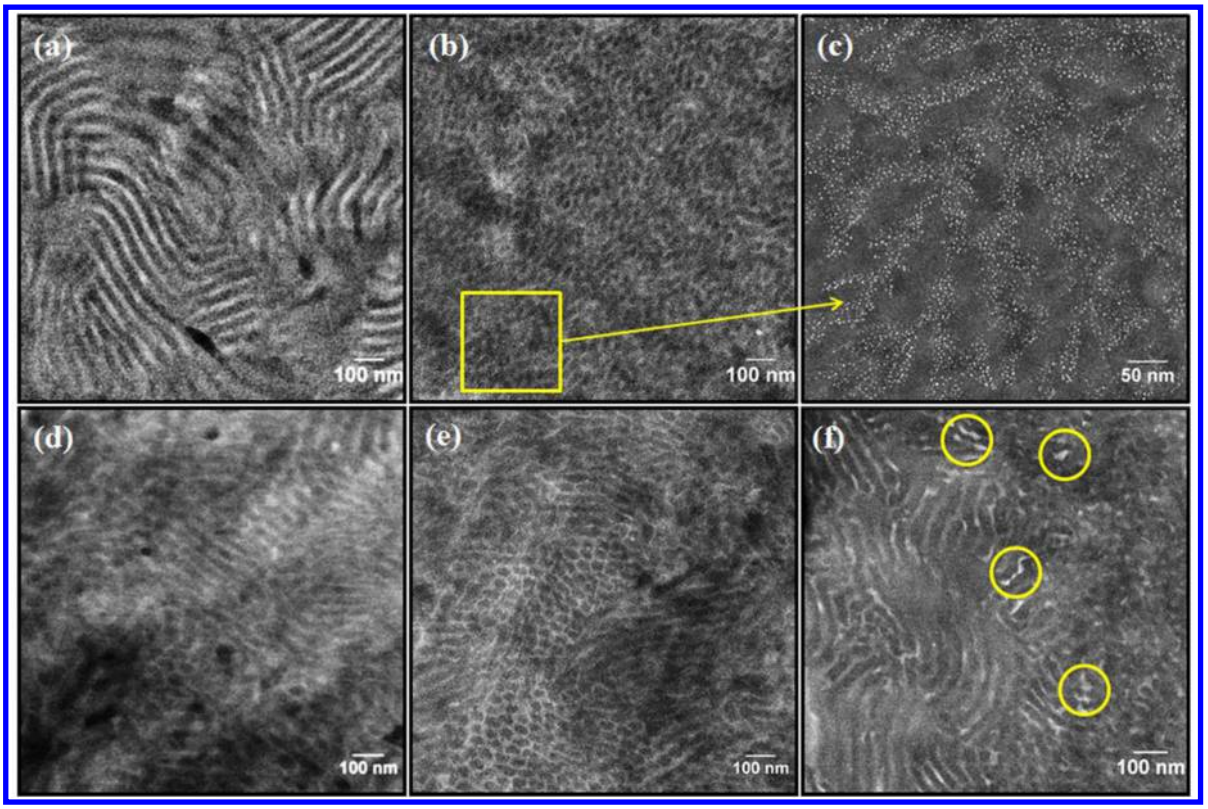

Figure 3. STEM images of SEO copolymer containing PEO-POSS nanoparticles (SEO-POSS-w_{POSS}) at different weight % of the inorganic portion of the nanoparticles (a) 0, (b, c) 2, (d) 5, (e) 7, and (f) 10.

the particle loading is increased further from 5 to 10 wt %. The high conductivity of SEO-LiTFSI-POSS-2 can, in principle, be due to two reasons. The presence of nanoparticles may either lead to an increase in free ions, as proposed in ref 4, or affect the morphology factor of the conduction pathways, as seen in ref 7.

STEM images of salt-free samples (SEO-POSS-w_{POSS}) are shown in Figure 3. SEO-POSS-0 exhibits a lamellar morphology (Figure 3a). The addition of 2 wt % of nanoparticles results in the formation of a bicontinuous phase (Figure 3b). It may, at first glance, seem surprising that such as small concentration of nanoparticles can have such a large effect on morphology. However, the POSS nanoparticles have a substantial corona of PEO. It is noted in Table 2 that the volume fraction of nanoparticles in SEO-POSS-2, $\phi_{PEO\text{-}POSS}$, is 0.13. If we assume that the nanoparticles are located in the PEO-rich microphase, then the nanoparticles occupy a substantial fraction of this microphase. A high resolution STEM image of SEO-POSS-2, corresponding to the region inside the square in Figure 3b, is shown in Figure 3c. In Figure 3c, we see bright nanoparticles with an average diameter of about 2.5 nm distributed inside a bicontinuous phase. Since PEO chains are grafted on the POSS particles, we expect the particles to be located in the PEO-rich microphase. The bright regions seen in Figure 3b clearly indicate the presence of silsesquioxane nanoparticles. Further increase of nanoparticle loading to 5 wt % results in the reappearance of the lamellar phase, as shown in Figure 3d. However, a honeycomb-like morphology is also evident in Figure 3d (bottom left corner). Similar coexisting morphologies are seen when nanoparticle loading is 7 and 10 wt % (Figure 3e, f). We are not sure of the reason for the formation of coexisting phases at high particle loadings. One possibility is that the coexisting morphologies seen in Figures 3d, e, and f are caused by a non-uniform distribution of nanoparticles. In SEO-POSS-10, we did find regions that were extremely bright suggesting the presence of a higher-than-average concentration of nanoparticles. Some of these regions are circled in Figure 3f. (We did not see any evidence of macrophase separation of the nanoparticles into a separate phase.)

SAXS measurements were performed on non-salty (SEO-POSS-w_{POSS}) and salty (SEO-LiTFSI-POSS-w_{POSS}) hybrid block copolymer mixtures at two different temperatures: 25 °C, the temperature at which the morphology was studied by STEM, and 90 °C, the temperature at which conductivity was measured. In Figure 4a, we show SAXS profiles of the non-salty samples. At 25 °C, the SAXS profile of SEO-POSS-0 is consistent with that expected from a lamellar morphology. We see a primary SAXS peak at $q = q^* = 0.084$ nm^{-1}. In addition, we see a third order peak at $q = 3q^* = 0.252$ nm^{-1}. The second order peak at $q = 2q^*$ is missing because the volume fraction of PEO in the block copolymer is nearly 0.5. Increasing the temperature of SEO-POSS-0 has little effect on the primary SAXS peak, but the high order peak at $3q^*$ vanishes (Figure 4a). It is likely that this is due to the reduction of the scattering contrast between the PEO-rich and PS-rich microphases; we note that PEO is crystalline at room temperature. The SAXS profile of SEO-POSS-2 contains a primary peak at about $q = q^* = 0.093$ nm^{-1} and no higher order peaks, consisting with the presence of disordered bicontinuous phases. The SAXS data of SEO-POSS-2 is consistent with STEM images (Figure 4a and Figure 3b).

SAXS profiles of SEO-POSS-5, SEO-POSS-7, and SEO-POSS-10 at 25 °C contain primary scattering peaks in the

DOI: 10.1021/ma502234y
Macromolecules 2015, 48, 358−364

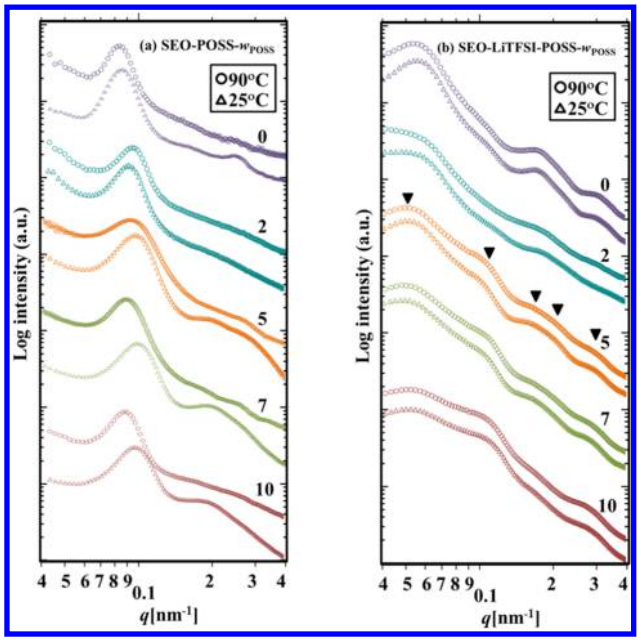

Figure 4. SAXS profiles of (a) non-salty (SEO-POSS-w_{POSS}) and (b) salty (SEO-LiTFSI-POSS-w_{POSS}) samples with different weight % of the inorganic portion of the nanoparticles, w_{POSS}, at 25 °C and at 90 °C. The arrows indicate Bragg reflections of q^*, $2q^*$, $3q^*$, $4q^*$, and $5q^*$ peaks.

vicinity of $q = q^* = 0.097$ nm^{-1} and broad shoulders in the vicinity of $q = 2q^*$ and $q = 3q^*$ (Figure 4a). These high order features suggest the formation of ordered phases (as opposed to bicontinuous phase). This is consistent with the STEM images shown in Figure 3. SAXS profiles of SEO-POSS-5, SEO-POSS-7, and SEO-POSS-10 at 90 °C do not contain higher order scattering peaks, consistent with observations on SEO-POSS-0 at 90 °C.

In Figure 4b, we show SAXS profiles of the salty samples. Both at 25 and 90 °C, the SAXS profiles of SEO-LiTFSI-POSS-0 indicate the presence of a lamellar morphology. We see a primary SAXS peak at $q = q^* = 0.057$ nm^{-1} and high order peaks at $q = 3q^* = 0.171$ nm^{-1} and $q = 5q^* = 0.285$ nm^{-1}. As for SEO-POSS-0, the peaks at $q = 2q^*$ and $q = 4q^*$ are missing in SEO-LiTFSI-POSS-0. The SAXS profiles of SEO-LiTFSI-POSS-2 in the low q limit are consistent with profiles expected from disordered bicontinuous phases. The SAXS profiles of SEO-LiTFSI-POSS-2 contain a broad shoulder at $q = 0.181$ nm^{-1}. The origin of this feature is unclear.

SAXS profiles of SEO-LiTFSI-POSS-5 at 25 °C contain a primary scattering peak in the vicinity of $q = q^* = 0.053$ nm^{-1} and high order peaks in the vicinity of $q = 2q^*$, $q = 3q^*$, $q = 4q^*$, and $q = 5q^*$; the expected location of the higher order peaks are indicated by arrows in Figure 4b. SAXS profile of SEO-LiTFSI-POSS-5 at 90 °C is similar to that at 25 °C, but the scattering features are less pronounced.

Increasing the nanoparticle concentration to 7 wt % results in virtually no change in the locations of the primary and higher order peaks, but the peak intensities are suppressed. The SAXS profiles of SEO-LiTFSI-POSS-10 are similar to those of SEO-LiTFSI-POSS-7 except for the further suppression of primary scattering peaks.

The domain spacing from SAXS of non-salty and salty samples, d_{SAXS}, given by $d_{SAXS} = 2\pi/q^*$ is plotted as a function of the weight fraction of nanoparticles in Figure 5. The addition

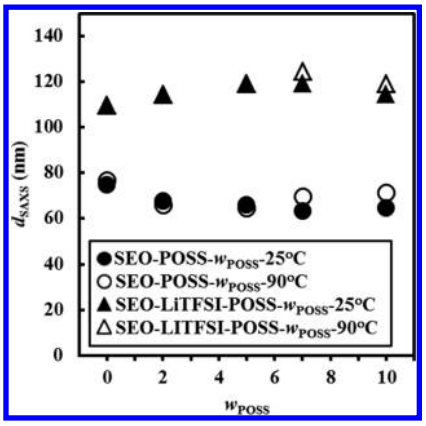

Figure 5. Domain spacing, d_{SAXS}, of non-salty (SEO-POSS-w_{POSS}) and salty (SEO-LiTFSI-POSS-w_{POSS}) samples versus weight % of the inorganic portion of the nanoparticles, w_{POSS}, at 25 °C and at 90 °C.

of 2 wt % nanoparticles in SEO-POSS-2 results in the decrease of d_{SAXS} in non-salty samples and an increase in the salty samples. Further increase of the nanoparticle concentration has no effect on d_{SAXS} in both non-salty and salty samples. The domain spacing of salty samples (SEO-LiTFSI-POSS-w_{POSS}) is higher than non-salty samples (SEO-POSS-w_{POSS}), regardless of the temperature. This can be interpreted as an increase of the effective segregation between PS and PEO domains due to the presence of LiTFSI.[25]

In Figure 6, we plot the conductivity, σ, of salty hybrid electrolyte samples at 90 °C as a function of the nanoparticle

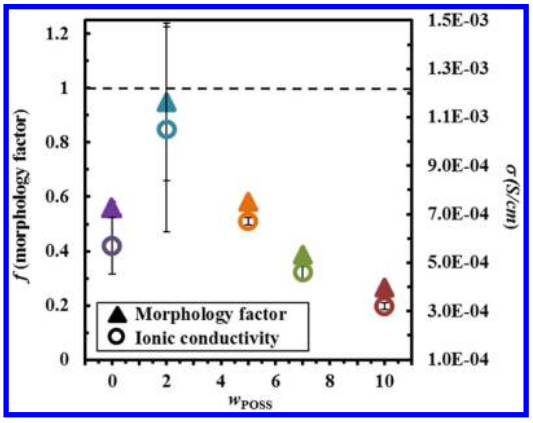

Figure 6. Morphology factor, f, and the ionic conductivity, σ, versus the weight % of the inorganic portion of the nanoparticles, w_{POSS}, of salty hybrid block copolymer samples (SEO-LiTFSI-POSS-w_{POSS}) at 90 °C. The dashed line corresponds to f_{ideal} and the expected maximum ionic conductivity for this block copolymer electrolyte.

weight fraction. The non-monotonic dependence of σ on nanoparticle weight fraction can be anticipated from Figure 2. These data can be used to calculate the morphology factor, f, using eq 1 where $\sigma(T)$ is the conductivity of the salty hybrid block copolymer samples (SEO-LiTFSI-POSS-w_{POSS}) and ϕ_c is the volume fraction of the PEO segments in the hybrid electrolyte. ($\phi_c = \phi_{EO}$, see Table 3.) Note that both the corona of the nanoparticles and the block copolymer chains contribute to the volume fraction of PEO segments. We ignore the volume occupied by unfunctionalized POSS nanoparticles because it is well-known POSS is non-conductor for lithium salts. The error introduced due to this approximation is small as the volume

DOI: 10.1021/ma502234y
Macromolecules 2015, 48, 358−364

occupied by the inorganic particles is 5.7 % or less; it is 1.4 % in the optimized electrolyte. The conductivity of PEO homopolymer electrolytes with molecular weights greater than 5 kg/mol is independent of the molecular weight.[26,27] We assume that the intrinsic conductivity of PEO-rich microphase, $\sigma_c = 1.86 \times 10^{-3}$ S/cm for r = [Li]/[EO] = 0.085 at 90 °C, the value obtained in high molecular weight PEO homopolymers.[28] This enables determination of f, and the results are shown in Figure 6.

The value of f for SEO-LiTFSI-POSS-0 is 0.55, close to the value expected for lamellar phases.[10] In contrast, the value of f for SEO-LiTFSI-POSS-2 is 0.94 ± 0.28, close to unity, the value expected for an idealized bicontinuous phase. Increasing w_{POSS} further beyond 2 wt % results in the reappearance of ordered lamellae and a concomitant decrease in f, as expected (Figure 4b). It is evident that f of SEO-LiTFSI-POSS-2 is significantly higher than previously reported morphology factors given in Table 1. Further work is required to uncover the reasons for this observation.

Our analysis assumes that the addition of POSS nanoparticles has no effect on transport through the PEO microphase. It is known that ion transport is affected by the glass transition temperature, T_g, of the conducting phase. DSC measurements were used to determinate T_g of our composite electrolytes. The results of these experiments are given in Table 3. T_g is the monotonic function of particle concentration, decreasing from −40 °C to −44 °C when the particle loading is increased from 0 to 2 wt %, and from −44 °C to −47 °C when loading is further increased from 2 to 10 wt %. It is likely that this effect is due to the fact that the molecular weight of the PEO chains attached to the nanoparticles is smaller than that of the SEO block copolymer. We are not aware of any methodology for accounting for the effect of the presence PEO chains tethered to nanoparticles on intrinsic conductivity. Our analysis thus uses measurements in pure PEO for normalization. It is clear, however, that the non-monotonic dependence of the conductivity on nanoparticle loading is not dominated by T_g which is a monotonic function of nanoparticle loading.

4. CONCLUSIONS

We have studied the effect of adding nanoparticles on the ionic conductivity of a block copolymer electrolyte. The addition of 2 wt % nanoparticles results in a surprising increase in ionic conductivity. Further increase of the nanoparticle loading decreases the ionic conductivity of the hybrid electrolytes. We use SAXS and STEM to show that the increase in ionic conductivity is due to a lamellar-to-bicontinuous phase transition. The magnitude of the increase in conductivity is consistent with the prevailing model that relates conductivity and morphology. The conductivity of the optimized hybrid electrolytes is only 6% lower than that of an ideal nanostructured electrolyte conducting pathways and no dead ends, i.e., the morphology factor is 0.94 ± 0.28. The morphology factor obtained in the optimized hybrid electrolyte in this study is higher than values reported in previous publications.[7,12−15]

AUTHOR INFORMATION

Corresponding Author

*Phone: (510) 642-8937. E-mail: nbalsara@berkeley.edu,

Notes

The authors declare no competing financial interest.

ACKNOWLEDGMENTS

This work was supported as part of the Joint Center for Energy Storage Research, an Energy Innovation Hub funded by the U.S. Department of Energy (DOE), Office of Science, Basic Energy Sciences (BES). X-ray scattering research at the Advanced Light Source was supported by DOE, Office of Science, BES. STEM work was provided by the Electron Microscopy of Soft Matter Program from the Office of Science, Office of Basic Energy Sciences, Materials Sciences and Engineering Division of the U.S. Department of Energy under Contract No. DE-AC02-05CH11231. The STEM experiments were performed as user projects at the National Center for Electron Microscopy, Lawrence Berkeley National Laboratory, under the same contract. We acknowledge Eric Schaible for beamline support. We would also like to thank Jacob L. Thelen for helpful comments on small-angle X-ray scattering measurements.

ABBREVIATIONS

PS	polystyrene
PEO	poly(ethylene oxide)
SEO	polystyrene-*b*-poly(ethylene oxide)
DMF	*N*,*N*-dimethylformamide
LiTFSI	lithium bis(trifluoromethanesulfone)imide
PEO-POSS	polyethylene glycol polyhedral oligomeric silsesquioxane
EO	ethylene oxide
SEO-POSS-w_{POSS}	non-salty hybrid block copolymers
SEO-LiTFSI-POSS-w_{POSS}	salty hybrid block copolymers
M_{PS}	molar mass of polystyrene
M_{PEO}	molar mass of poly(ethylene oxide)
M_s	molar mass of styrene
M_{EO}	molar mass of ethylene oxide
$\rho_{PEO\text{-}POSS}$	density of PEO-POSS nanoparticles
$w_{EO(SEO)}$	weight percentage of EO in SEO copolymer
w_{POSS}	weight percentage of inorganic content (POSS)
$w_{PEO\text{-}POSS}$	weight percentage of PEO-POSS nanoparticles
$w_{EO(PEO\text{-}POSS)}$	weight percentage of EO in the PEO-POSS nanoparticles
v_{LiTFSI}	molar volume of LTFSI
v_S	molar volume of styrene monomer units
v_{EO}	molar volume of ethylene oxide monomer units
ϕ_{EO}	volume fraction of conducting phase in the hybrid electrolytes
ϕ_{POSS}	volume fraction of inorganic content (POSS)
$\phi_{PEO\text{-}POSS}$	volume fraction of PEO-POSS nanoparticles
$\sigma(T)$	conductivity of hybrid electrolytes
f	morphology factor
$\sigma_c(T)$	intrinsic conductivity of conducting phase
l	thickness
S	area
R_{el}	electrolyte resistance

DOI: 10.1021/ma502234y
Macromolecules 2015, 48, 358−364

r	molar ratio of lithium atoms to EO moieties
d_{SAXS}	domain spacing from SAXS of non-salty and salty samples

REFERENCES

(1) Parker, J. M.; Wright, P. V. *Polymer* **1973**, *14*, 589.
(2) Lascaud, S.; Perrier, M.; Vallee, A.; Besner, S.; Prud'homme, J.; Armand, M. *Macromolecules* **1994**, *27*, 7469−7477.
(3) Armand, M. *Annu. Rev. Mater. Res.* **1986**, *16*, 245−261.
(4) Croce, F.; Appetecchi, G. B.; Persi, L.; Scrosati, B. *Nature* **1998**, *394*, 456−458.
(5) Soo, P. P.; Huang, B.; Jang, Y.; Chiang, Y. M.; Sadoway, D. R.; Mayes, A. M. *J. Electrochem. Soc.* **1999**, *146*, 32−37.
(6) Cochran, E. W.; Garcia-Cervera, C. J.; Fredrickson, G. H. *Macromolecules* **2006**, *39*, 2449−2451.
(7) Singh, M.; Odusanya, O.; Wilmes, G. M.; Gomez, E. D.; Patel, A. J.; Chen, V. L.; Park, M. J.; Eitouni, H. B.; Fragouli, P.; Iatrou, H.; Hadjichristidis, N.; Balsara, N. P. *Macromolecules* **2007**, *40*, 4578−4585.
(8) Teran, A. A.; Mullin, S. A.; Hallinan, D. T.; Balsara, N. P. *ACS Macro Lett.* **2012**, *1*, 305−309.
(9) Young, W. S.; Kuan, W. F.; Epps, T. H. *J. Polym. Sci., Part B: Polym. Phys.* **2014**, *52*, 1−16.
(10) Hallinan, D. T.; Balsara, N. P. *Annu. Rev. Mater. Res.* **2013**, *43*, 503−525.
(11) Sax, J.; Ottino, J. M. *Polym. Eng. Sci.* **1983**, *23*, 165−176.
(12) Weber, R. L.; Ye, Y.; Schmitt, A. L.; Banik, S. M.; Elabd, Y. A.; Mahanthappa, M. K. *Macromolecules* **2011**, *44*, 5727−5735.
(13) Wanakule, N. S.; Panday, A.; Mullin, S. A.; Gann, E.; Hexemer, A.; Balsara, N. P. *Macromolecules* **2009**, *42*, 5642−5651.
(14) Schulze, M. W.; McIntosh, L. D.; Hillmyer, M. A.; Lodge, T. P. *Nano Lett.* **2014**, *14*, 122−126.
(15) Hamersky, M. W.; Hillmyer, M. A.; Tirrell, M.; Bates, F. S.; Lodge, T. P.; von Meerwall, E. D. *Macromolecules* **1998**, *31*, 5363−5370.
(16) Warren, S. C.; DiSalvo, F. J.; Wiesner, U. B. *Nat. Mater.* **2007**, *6*, 156−161.
(17) Lin, Y.; Daga, V. K.; Anderson, E. R.; Gido, S. P.; Watkins, J. J. *J. Am. Chem. Soc.* **2011**, *133*, 6513−6516.
(18) Wu, Y. R.; Wu, Y. C.; Kuo, S. W. *Macromol. Chem. Phys.* **2013**, *214*, 1496−1503.
(19) Chiu, J. J.; Kim, B. J.; Kramer, E. J.; Pine, D. J. *J. Am. Chem. Soc.* **2005**, *127*, 5036−5037.
(20) Jang, S. G.; Audus, D. J.; Klinger, D.; Krogstad, D. V.; Kim, B. J.; Cameron, A.; Kim, S. W.; Delaney, K. T.; Hur, S. M.; Killops, K. L.; Fredrickson, G. H.; Kramer, E. J.; Hawker, C. J. *J. Am. Chem. Soc.* **2013**, *135*, 6649−6657.
(21) Kim, B. J.; Fredrickson, G. H.; Hawker, C. J.; Kramer, E. J. *Langmuir* **2007**, *23*, 7804−7809.
(22) Mullin, S. A.; Stone, G. M.; Panday, A.; Balsara, N. P. *J. Electrochem. Soc.* **2011**, *158*, A619−A627.
(23) Yuan, R.; Teran, A. A.; Gurevitch, I.; Mullin, S. A.; Wanakule, N. S.; Balsara, N. P. *Macromolecules* **2013**, *46*, 914−921.
(24) Patel, S. N.; Javier, A. E.; Stone, G. M.; Mullin, S. A.; Balsara, N. P. *ACS Nano* **2012**, *6*, 1589−1660.
(25) Panday, A.; Mullin, S.; Gomez, E. D.; Wanakule, N.; Chen, V. L.; Hexemer, A.; Pople, J.; Balsara, N. P. *Macromolecules* **2009**, *42*, 4632−4637.
(26) Teran, A. A.; Tang, M. H.; Mullin, S. A.; Balsara, N. P. *Solid State Ionics* **2011**, *203*, 18−21.
(27) Hayamizu, K.; Akiba, E.; Bando, T.; Aihara, Y. *J. Chem. Phys.* **2002**, *117*, 5929−5939.
(28) Lascaud, S.; Perrier, M.; Vallee, A.; Besner, S.; Prud'homme, J.; Armand, M. *Macromolecules* **1994**, *27*, 7469−7477.

DOI: 10.1021/ma502234y
Macromolecules 2015, 48, 358−364